PCCP

PAPER

View Article Online
View Journal | View Issue

Cite this: *Phys. Chem. Chem. Phys.*, 2025, **27**, 16558

Tailored solution environment for protein crystallization: tuning solubility, nucleation, and growth by urea and salt

T. Hamacher[a] and F. Platten *[ab]

Received 28th April 2025,
Accepted 14th July 2025

DOI: 10.1039/d5cp01614b

rsc.li/pccp

Urea has recently been shown to modulate protein–protein interactions at sub-denaturing concentrations (M. Madani *et al. Soft Matter* 2025, **21**, 1937–1948). Here, we investigate how urea and salt together influence protein crystallization by tuning both thermodynamic and kinetic parameters. Solubility, a key thermodynamic property, is affected differently by the two additives: urea increases lysozyme solubility, while sodium chloride decreases it without inducing a salting-in effect. When solubility is plotted as a function of the second virial coefficient (B_2), the data collapse onto a master curve. From these measurements, we calculate the chemical potential difference ($\Delta\mu$) between solution and crystal, generating a $\Delta\mu$ map across the phase diagram. Crystallization kinetics at selected points were monitored using video microscopy. Salt reduces the induction time and accelerates crystal growth, whereas urea produces the opposite effect. The dependencies of the kinetic parameters on $\Delta\mu$ are described by classical nucleation theory and a birth-and-spread growth model, respectively. Strikingly, urea enables crystallization at lower supersaturation levels, and at a fixed $\Delta\mu$, enhances both nucleation and growth compared to salt alone. Overall, our results reveal how urea and salt independently govern thermodynamic and kinetic factors. We propose that tuning the solution environment through salt and nonspecific additives such as urea provides a general strategy to optimize crystallization conditions for globular proteins.

1. Introduction

Protein condensation is a critical process in both biological systems and materials science.[1–8] It plays a central role in phenomena such as crystallization,[9,10] fibril formation,[11,12] and liquid–liquid phase separation (LLPS).[13] These condensed states are not only essential in biological processes, including protein aggregation and disease (*e.g.*, Alzheimer's, Parkinson's, amyloidosis), but also hold significant potential for applications in biotechnology, drug discovery, and material design. Controlling protein condensation, whether through solution conditions[14–16] or by applying external fields,[17–20] opens up possibilities for designing new biomaterials and advancing protein-based therapeutics.

Protein crystallization, one of the most studied forms of protein condensation, is a cornerstone technique in structural biology that enables the determination of protein structures at atomic resolution.[9,21,22] Despite its importance, optimizing crystallization conditions remains a challenge, often relying on trial-and-error approaches.[23] This challenge stems from the complex behavior of proteins in solution, where intermolecular interactions depend on the specific protein, solvent conditions, and additives. A more comprehensive understanding of the physical principles behind protein crystallization is essential to streamline this process, reduce empirical experimentation, and improve the success rate of crystallization efforts.[10]

Protein crystallization involves a delicate balance of thermodynamic and kinetic factors. Thermodynamically, proteins can crystallize when their concentration exceeds the equilibrium solubility, a condition that can be achieved, for example, through changes in temperature or pH, or by adding solution additives or precipitants.[24] In particular, when solubility is low, proteins tend to remain undissolved or aggregate in solution, making it difficult to isolate them in a functional and stable form. Thus, low solubility poses significant challenges in fields such as structural biology, drug development, and biotechnology.[25] In structural biology, it hinders the use of techniques like X-ray crystallography and NMR spectroscopy. In drug development, poor solubility complicates the formulation of stable protein-based therapeutics. Additionally, low solubility can cause aggregation and instability during protein purification and reduce enzyme efficiency in industrial applications like food processing.

[a] *Faculty of Mathematics and Natural Sciences, Heinrich Heine University Düsseldorf, 40225 Düsseldorf, Germany. E-mail: florian.platten@hhu.de*
[b] *Institute of Biological Information Processing IBI-4, Forschungszentrum Jülich, 52428 Jülich, Germany*

Protein crystallization kinetics studies the rates and mechanisms governing the formation and growth of protein crystals. While crystallization can proceed *via* different pathways,[26] nucleation marks the first step in forming an ordered crystal lattice. It involves the spontaneous formation of small clusters of protein molecules that transition into stable nuclei capable of growing into larger crystals. Direct measurement of nucleation is challenging because the initial nuclei are too small and short-lived to be observed directly by light microscopy. Therefore, nucleation is often inferred indirectly using techniques such as optical microscopy, which detects small crystals once they have grown large enough to be visible, or light scattering, where the intensity increases sharply as soon as crystals begin to form. From these observations, the induction time, defined as the delay between reaching supersaturation and the first detectable crystal formation, can be estimated. This induction time varies widely depending on the protein and specific solution conditions. Alternative approaches to determine nucleation rates more directly, such as the double-pulse technique,[27–30] aim to separate nucleation and growth processes by rapidly shifting the system between high and low supersaturation. While more demanding in terms of experimental setup, these methods have yielded valuable insights, particularly in systems where crystal growth significantly affects supersaturation. Since nucleation marks the onset of crystallization, the subsequent stage – crystal growth – follows as protein monomers or assembled units become incorporated into the crystal lattice, although additional nucleation events may still occur during this stage. However, the rate of growth can be influenced by solution composition and temperature, and growth often slows or even ceases if supersaturation decreases or if ripening occurs. Despite advances in understanding crystallization kinetics,[21,31–34] there are still significant challenges, such as accurately predicting induction times, optimizing growth rates, and preventing unwanted phenomena like aggregation or polymorphism, all of which can hinder the reproducibility and quality of the final crystals.

Solution additives or precipitants are commonly used to modify the solution environment, altering solubility and other physicochemical properties, which in turn can promote crystallization.[35–39] Proteins may also be chemically modified to enhance their solubility.[40,41] While salts, polyethylene glycol (PEG), and organic solvents have been extensively studied in this context, urea has received comparatively less attention.[42] Urea is a well-known protein denaturant at high concentrations and has been widely used to study protein folding and unfolding.[43–55] By disrupting non-covalent interactions such as hydrogen bonds, hydrophobic forces, and electrostatic interactions, urea promotes protein unfolding and alters the solvation properties of proteins.

However, the effects of urea on proteins and their assemblies at lower, sub-denaturing concentrations remain poorly understood. At these concentrations, urea may still modulate protein–protein interactions and influence crystallization. The precise mechanisms remain unclear but may involve modifications to the physicochemical environment, such as dielectric properties and subtle alterations in hydration, which in turn affect intermolecular interactions, protein solubility, and potentially transport properties. For example, urea has been shown to reduce the amount of protein bound to interfaces.[56,57] Since adsorbed protein films often behave as dense systems where protein–protein interactions are significant, the reduced surface excess upon urea addition suggests that urea may modulate these interactions, affecting condensed states. The effect of urea on LLPS, particularly its role in lowering cloud-point temperatures, has been recently highlighted,[58] underscoring the broader significance of chemical denaturants in protein phase transitions. A theoretical study on crystal growth[59] suggested that denaturants might promote crystallization by destabilizing non-productive protein interactions with crystal surfaces, where proteins bind in incorrect, non-crystalline orientations. However, to our knowledge, this hypothesis has not been tested experimentally. Although high concentrations of urea are commonly used for protein denaturation, and its effects on condensed protein states are established, systematic experimental investigations into its influence on protein crystallization and the underlying mechanisms remain lacking.

In our previous study,[60] we explored the lysozyme state diagram and protein interactions in the presence of urea and salt, attributing the impact of urea primarily to alterations in the dielectric properties of the solution. In this work, we extend these findings by examining the combined effects of urea and salt on lysozyme crystallization, focusing on how they influence the thermodynamics and kinetics of crystallization. We systematically investigate their impact on protein solubility and provide a preliminary analysis of their effects on nucleation and growth. While sodium chloride decreases solubility without a salting-in effect, urea increases solubility. Protein interactions in the presence of both urea and salt are quantified using the second virial coefficient (B_2). We show that the solubility data collapse onto a master curve when plotted as a function of B_2, independent of urea and salt concentrations, underscoring the crucial role of these interactions in determining solubility. From the solubility data, we construct a map of the chemical potential difference $\Delta\mu$ for the state diagram. The chemical potential difference, which drives crystallization, increases logarithmically with salt concentration and decreases linearly with urea content. Crystallization kinetics, studied through video microscopy, reveal that the induction time decreases with salt concentration and increases with urea concentration, while crystal growth rates exhibit the opposite trends. However, when compared at a fixed $\Delta\mu$, urea can promote both nucleation and growth. It is conceivable that the addition of urea lowers the energy barrier for nucleation and suppresses non-productive binding to the growing crystal, leading to increased nucleation and growth rates compared to the presence of sodium chloride alone at the same supersaturation level. Furthermore, crystallization occurs at lower supersaturations in the presence of urea. The observed behaviors can be described in terms of classical nucleation theory and a birth-and-spread growth model, respectively. These results offer new insights into the physical processes governing protein crystallization and lay a foundation for optimizing crystallization conditions by

independently tuning thermodynamics and kinetics through the careful selection of salt and nonspecific additives. We propose that combining salts with nonspecific additives, such as urea, provides a general strategy for fine-tuning the solution environment and modulating protein interactions, thereby improving crystallization conditions for globular proteins.

2. Experimental section

2.1. Sample preparation

Samples for batch crystallization experiments were prepared following the procedure outlined in detail previously,[61] with essential steps summarized here. Lysozyme (Sigma-Aldrich, prod. no. L6876), sodium chloride (NaCl; Fisher Scientific, prod. no. S/3160/60), urea (Merck, prod. no. 1.08488; Sigma, prod. no. 33247), and sodium acetate (NaAc; Merck, prod. no. 1.06268) were used as received. All buffer solutions were prepared using ultrapure water with a resistivity of 18.2 MΩ cm. Lysozyme powder was dissolved in 50 mM sodium acetate buffer, and the pH was adjusted to 4.5 by adding hydrochloric acid. The resulting protein solution, typically at a concentration of 80 mg mL^{-1}, was filtered multiple times through an Acrodisc syringe filter (Pall, prod. no. 4611) with a 0.1 μm pore size, designed to minimize protein binding, to remove impurities and undissolved aggregates. For more concentrated solutions, the protein solution was further concentrated using a stirred ultrafiltration cell (Amicon, Millipore, prod. no. 5121) with an Omega 10 kDa membrane disc filter (Pall, prod. no. OM010025), and the resulting retentate served as the concentrated protein stock. The concentration of the stock solution was determined using UV/vis spectroscopy and refractometry. Salt and urea stock solution concentrations were measured using refractometry and compared to literature values.[44,62] Due to the hygroscopic nature of urea, precise measurements of additive concentrations were crucial when preparing concentrated urea stock solutions. Samples were prepared by accurately pipetting defined volumes of buffer, protein, salt, and urea stock solutions at ambient temperature.

2.2. Solubility measurements

For batch crystallization, supersaturated protein samples, initially at concentrations of 20 mg mL^{-1} or 80 mg mL^{-1}, were incubated at (18.9 ± 0.2) °C for at least 150 days to allow equilibration. Protein crystals were visibly observed in most cases after this period. Protein solubility (c_{eq}) was then determined by measuring the protein concentration of the supernatant in equilibrium with protein crystals, as in previous studies.[63–66] For each condition, two to three independent samples were prepared. After incubation, the protein concentration in the supernatant was measured spectrophotometrically[67] at 280 nm following dilution in buffer, using a specific absorption coefficient of 2.64 mL mg^{-1} cm^{-1}. Absorbance measurements were repeated at least three times per sample, with results averaged. For some conditions, the refractive index of the supernatant was monitored in addition (data not shown). A constant plateau value was typically reached after approximately 50 days and remained stable thereafter, clearly confirming that equilibrium had been established. This stable concentration over time is the widely accepted criterion for determining solubility from crystallization experiments.[24,68,69] Early studies demonstrated that both crystallization from a supersaturated solution and dissolution into an undersaturated solution converge toward the same asymptotic equilibrium concentration.[70] Today, both methods are considered valid, provided equilibration is confirmed by such stable concentration plateaus. Our equilibration time and approach align well with previous observations,[71] where the initial protein concentration was chosen to initiate crystallization within a reasonable timeframe and with an appropriate number of nuclei, as in our work.

2.3. Optical microscopy to follow protein crystallization *in situ*

Crystallizing samples were monitored *in situ* using bright-field optical microscopy. Custom-designed sample cells consisted of a microscope slide and three cover slips. Two cover slips served as spacers, creating a gap, while the third was placed on top to form a narrow capillary chamber. The sample solution was introduced into the chamber, and the cell was sealed with UV-curing adhesive. The sample cell was then mounted on the stage of a Laborlux S microscope (Leitz), equipped with a 25× objective and a Stingray F-504C (AVT) camera. Samples were prepared with an initial protein concentration of 20 mg mL^{-1} and various salt and urea concentrations. Time-lapse series of microscope images were recorded at a rate of one frame per minute, starting as soon as crystals appeared in the field of view. For each solution composition, the formation of at least six crystals with clearly identifiable crystal faces, each grown from independently prepared solutions, was monitored and analyzed. Microscopy experiments were conducted at (19 ± 1) °C.

2.4. Estimation of kinetic parameters: the crystallization induction time and the crystal growth rate

The onset of crystallization is often inferred from changes of the supernatant concentration, measured spectrophotometrically,[72] or from increased light scattering.[63] Optical microscopy, however, provides a more direct and visual observation of crystal formation.[73] The crystallization induction time (t_{ind}) is defined as the elapsed time after sample preparation until the first crystal becomes visible under the microscope,[74] with a detection limit of approximately 2–3 μm.

Our sample volume of roughly 20 μL lies between typical bulk crystallization and microfluidic droplets, where stochastic nucleation remains relevant. Accordingly, nucleation events in such volumes follow a Poisson process, making the induction time t_{ind} a random variable representing the probabilistic waiting time for the first detectable nucleus. We report the mean induction time across replicates as a robust kinetic measure.[75]

Initial crystal face growth rates (G) were determined from the time-lapse series of microscope images.[65] For crystals with appropriate orientation (viewing direction perpendicular to the (110) face or along the four-fold symmetry axis, and not too closely packed), the size of the crystal faces was analyzed using

ImageJ software and plotted as a function of time after sample preparation. Initially, a constant growth rate was observed, which later decreased as the crystals grew larger and protein depletion occurred, a trend also reported in previous studies.[76] Growth rates for the (110) and (101) faces, G_{110} and G_{101}, were calculated as described by Durbin and Feher.[77]

3. Results and discussion

3.1. State diagram

In a previous study,[60] we investigated the state diagram of lysozyme at a fixed protein concentration of 20 mg mL^{-1}, across a range of urea and salt concentrations. For simplicity, Fig. 1a shows only the schematic state boundaries, omitting detailed experimental conditions. The diagram highlights the regions in which lysozyme forms a homogeneous solution, crystallizes, or undergoes metastable LLPS. The addition of urea increases the required NaCl concentration to induce the various condensed states.

Crystallization and LLPS are favored if attractive interactions in protein solution prevail.[78–81] Therefore, the increased salt concentration in the presence of urea suggests that urea weakens the attractive interactions, while NaCl, by screening electrostatic repulsion between proteins, is expected to enhance attraction.

These findings align with the previous work,[60] which involved a systematic analysis of SAXS data of protein solutions. Furthermore, the DLVO theory was shown to quantitatively describe the observed trends in interactions. This suggests that salt affects the system primarily through screening effects, while urea alters the dielectric properties of the solution, thereby influencing the van der Waals forces between proteins. Non-DLVO effects, such as hydration, hydrogen bonding, and the hydrophobic effect, were effectively accounted for by a constant cut-off length in the calculation of the second virial coefficient, independent of the urea and salt concentrations.

Fig. 1b shows representative microscope images for various solution conditions, again as a function of urea and salt concentration. The images were taken several days or weeks after preparation, showing the final crystal states when no further microscopic changes are observed. Depending on the urea and salt concentrations, different shapes of tetragonal crystals and additional crystal morphologies (sea-urchin crystals) are observed. In the absence of urea, at 0.5 M NaCl, elongated tetragonal crystals are observed, while at 0.9 M and 1.3 M NaCl, symmetric or rhomboid-shaped crystals are seen. At 2.0 M NaCl, sea-urchin-like crystals appear, though they are not the focus of this study. On the other hand, for the series with 0.9 M NaCl and varying urea concentrations, it is notable that crystals become more elongated with increasing urea concentration. Thus, the effect of urea counteracts the effect of NaCl. At higher salt concentrations, this effect of urea is less pronounced, and cuboid or rhomboid crystals dominate. It is also observed for high salt concentrations that the edges of the crystals are sometimes slightly rounded, or the crystal surfaces appear roughened. Furthermore, the number and size of the crystals are modulated by the addition of both urea and salt.

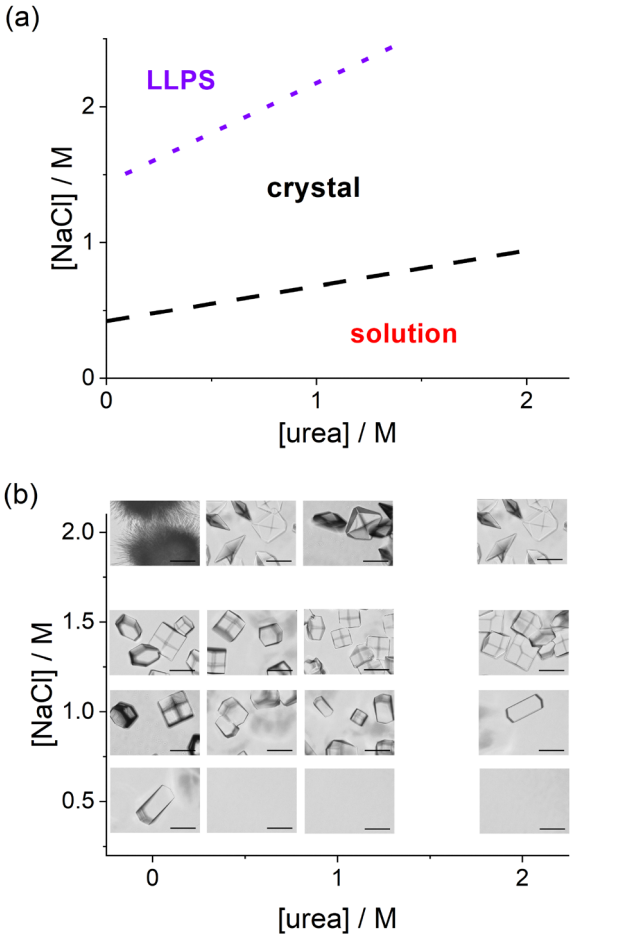

Fig. 1 State diagram. (a) Schematic state diagram of lysozyme solutions in the urea *vs.* salt concentration space (pH 4.5, room temperature, protein concentration 20 mg mL^{-1}), adapted from ref. 60. The diagram is based on measurements from a series of solutions with systematically varied urea and salt concentrations. For clarity, it shows approximate state boundaries, indicating regions of homogeneous solution, crystal–solution coexistence, and metastable LLPS. (b) Microscope images illustrating various shapes of tetragonal crystals and crystal morphologies in the state diagram (a) for various urea (0 M, 0.54 M, 1.1 M, 2 M) and salt concentrations (0.5 M, 0.9 M, 1.3 M, 2 M). The scale bar represents 50 μm.

Similar shapes of tetragonal crystals were observed in previous studies[65,77] when protein concentration was varied at a fixed NaCl concentration, or when salt concentration was varied at a fixed protein concentration. The different shapes of tetragonal lysozyme crystals were attributed to variations in the growth rates of the (110) and (101) faces of the crystals. In this context, elongated crystals could indicate a higher growth rate of the (101) face compared to the (110) face, while rhomboid crystals would imply a higher growth rate of the (110) face compared to the (101) face. It is reasonable to assume that the addition of urea could also have a modulating effect on the growth rates. For the series with 0.9 M NaCl and varying urea concentrations, this would suggest that the growth rate of the (101) face relative to that of the (110) face should increase with rising urea concentrations. Moreover, roughened crystals have also been observed at high salt concentrations before.[82]

The observations discussed in relation to Fig. 1 clearly indicate that urea likely not only modulates the state diagram and interactions of the proteins but also influences protein crystallization. The shift of the crystallization boundary (Fig. 1a) to higher salt concentrations with increasing urea concentration suggests an impact on the equilibrium solubility, a key parameter of crystallization thermodynamics. Note that the crystallization boundary is, in principle, a kinetic concept. It defines the solution conditions under which crystals spontaneously form on experimental time scales. Spontaneous crystal formation requires a certain level of supersaturation, and the lower this level, the longer one must wait for crystallization to occur. In contrast, the true equilibrium solubility corresponds to the maximum amount of protein that can dissolve at a given temperature, which is represented by a point on the liquidus line. The different crystal shapes and morphologies (Fig. 1b) as well as variations in the number and size of the crystals point to the modulation of crystallization kinetics by urea. In the following, we will analyze various aspects of the thermodynamics and kinetics of tetragonal lysozyme crystal formation in the presence of urea and salt in more detail.

3.2. Solubility

While the effects of NaCl and other salts on protein solubility have been extensively studied,[64,83–86] systematic studies on the effect of urea on lysozyme solubility are lacking. Fig. 2 shows the dependence of lysozyme solubility on urea and salt concentrations. Without urea, solubility decreases monotonically with increasing salt concentration, following a seemingly hyperbolic relationship. Similar behavior is observed for various fixed urea concentrations, although higher urea concentrations shift the curve as a whole to higher solubility values.

The solubility data in the absence of urea align with literature values. In the comprehensive study by Forsythe *et al.*,[64] lysozyme solubility was examined as a function of temperature, pH and salt concentration, though not at the temperature used in our study. Our results lie between the respective higher and lower temperature data from Forsythe *et al.*[64]

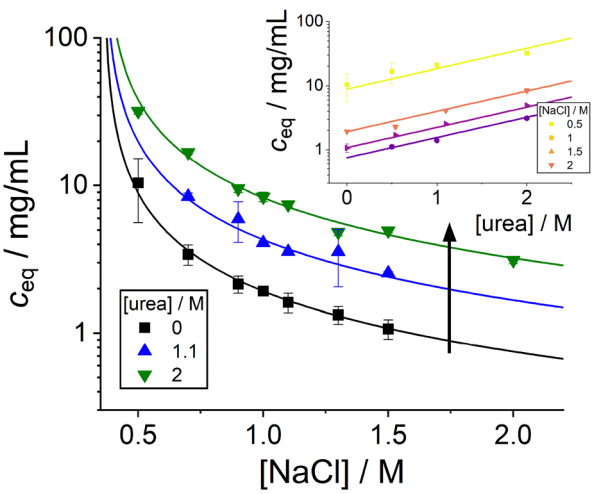

Fig. 2 Solubility (c_{eq}) of tetragonal lysozyme crystals as a function of NaCl concentration at various urea concentrations (as indicated): data (symbols) and global fits (lines) according to eqn (4). Increasing urea concentration is indicated by an arrow. (inset) Solubility (c_{eq}) of tetragonal lysozyme crystals as a function of urea concentration at different NaCl concentrations (as indicated): data (symbols) and global fits (lines) according to eqn (4).

The dependence of solubility on various additives, particularly salts, is often described by a heuristic approach. The logarithm of solubility is modeled as a linear function of additive concentration or ionic strength. This empirical approach, based on the work of Cohn[87] and Green,[88,89] is sometimes referred to as the Cohn–Green formula, which describes salting-out effects. In some cases, especially at low additive concentrations, an additional term dependent on the square root of the additive concentration or ionic strength is included to account for salting-in effects dominant at low concentrations. In agreement with previous work,[90] the monotonic decrease of solubility with NaCl content (Fig. 2) indicates the absence of a salting-in region. Moreover, c_{eq}, when plotted logarithmically as a function of salt concentration (Fig. 2), does not exhibit a linear relationship over large ranges of salt concentration. Salting-in effects are often attributed to dominant electrostatic interactions, while salting-out behavior is typically ascribed to the predominant hydrophobic effect,[91] with a primary focus on protein–additive interactions. In our case, however, protein–protein interactions likely play an important role as well (see Section 3.3), suggesting that solubility is governed primarily by the effective interactions between protein molecules, which are modulated by the nature of the additives.

A physically consistent and comprehensive theoretical framework for describing protein crystallization equilibria was introduced by Schmit and Dill.[92] They developed a many-body electrostatic model to describe the dependence of solubility on salt concentration, pH, and temperature. In their approach, the crystal is assumed to be macroscopically electrostatically neutral, with fixed charges on protein molecules balanced by a substantial enrichment of counterions. This counterion partitioning leads to an entropic penalty that opposes crystallization, while the resulting electrostatic screening favors stabilization *via* non-electrostatic interactions such as hydrophobic interactions and hydrogen bonding. This theory not only captures the dependence of solubility data on salt, pH and temperature but also explains thermodynamic signatures observed in calorimetric measurements.[93] While the Schmit–Dill theory could potentially be applied to our dataset, doing so would require computational efforts as well as additional knowledge of the effects of urea on hydration and the hydrophobic effect, or, alternatively, the introduction of more free fitting parameters. However, our goal here is to investigate whether the solubility dependence on additive composition can be described by a simple functional relationship, minimizing the number of parameters required for fitting.

Indeed, the data as a function of salt concentration at a fixed urea concentration can be described quantitatively by a simple hyperbolic relationship with only two independent parameters, a_s and b_s:

$$c_{eq}([salt])|_{urea}/c_0 = (a_s + b_s[salt])^{-1}, \quad (1)$$

where the vertical line with the subscript 'urea' indicates that solubility is considered at a fixed urea concentration and c_0

represents a reference concentration, set at 1 mg mL^{-1} here. For different urea concentrations, the term a_s needs to be adjusted, but the parameter b_s, which describes the dependence on salt concentration, can remain constant across urea concentrations.

Conversely, as shown in the inset of Fig. 2, solubility at fixed salt concentration increases linearly with urea concentration when plotted logarithmically. This can be quantitatively described using two free parameters, a_u and b_u, as follows:

$$\ln(c_{eq}([\text{urea}])|_{\text{salt}}/c_0) = a_u + b_u[\text{urea}], \quad (2)$$

where the vertical line with the subscript 'salt' indicates that solubility is considered at a fixed salt concentration. To align with subsequent analyses (*cf.* eqn (9)), we use the natural logarithm in eqn (2) instead of the decadic logarithm. This change only affects the numerical values of the parameters. For varying salt concentrations, the same slope b_u is observed, but different values for the intercept a_u are needed, depending on the salt concentration.

To motivate a universal expression for the solubility dependence on both salt and urea concentrations, we build on the individual empirical relationships for each component. Using eqn (2), we begin by considering the case where the urea concentration is zero, and relax the assumption of a constant salt concentration, as this equation should hold for any salt concentration. Under this condition, the parameter a_u can be identified with the natural logarithm of the solubility described in eqn (1), which depends solely on salt concentration:

$$a_u = \ln(c_{eq}([\text{salt}])|_{\text{urea}=0}/c_0) = -\ln(a_s + b_s[\text{salt}]). \quad (3)$$

This identification allows us to extend eqn (2) to arbitrary urea and salt concentrations, yielding a generalized expression that describes the solubility as a function of both salt and urea concentrations:

$$\ln(c_{eq}([\text{salt}],[\text{urea}])/c_0) = -\ln(a_s + b_s[\text{salt}]) + b_u[\text{urea}]. \quad (4)$$

A global fit of the dataset (lines in Fig. 2) yields the following parameter values:

$$a_s = -0.29 \pm 0.03, \quad b_s/M^{-1} = 0.81 \pm 0.03,$$
$$b_u/M^{-1} = 0.73 \pm 0.02.$$

The fact that solubility data can be heuristically described by such a simple equation with only few parameters may also be relevant for future studies, particularly in the field of crystallization kinetics, where solubility often needs to be known or interpolated for various conditions. Furthermore, eqn (4) expresses c_{eq} as a product of two separate factors, one depending only on urea concentration and the other only on salt concentration, with no factors that depend on both concentrations simultaneously. This functional form indicates that urea and salt influence solubility independently. The following section tests whether quantitative changes in protein–protein interactions under different solution conditions correlate with observed variations in solubility.

3.3. Interactions and solubility

The nature of the interactions between two particles, whether attractive or repulsive, is reflected in the sign of the second virial coefficient B_2, while its magnitude indicates the strength of the net interaction. For a spherosymmetric potential $U(r)$ with center-to-center distance r between two particles, B_2 is given by the following integral:

$$B_2 = 2\pi\int_0^\infty \left(1 - \exp\left[-\frac{U(r)}{kT}\right]\right) r^2 dr, \quad (5)$$

where kT is the thermal energy. Often, B_2 is normalized by the second virial coefficient of a hard-sphere reference system, $B_2^{HS} = \frac{2}{3}\pi\sigma^3$ with particle diameter σ, yielding $b_2 = B_2/B_2^{HS}$.

Earlier work has shown that the dependence of b_2 on urea and salt concentrations in lysozyme solutions can be quantitatively described using a Derjaguin–Landau–Verwey–Overbeek (DLVO) model in agreement with experimental data.[60] Within this framework, the addition of salt leads to a gradual decrease in the Debye screening length, reducing the range of electrostatic repulsion between protein molecules. This shift allows attractive forces to become more dominant, resulting in a net increase in overall attraction. In contrast, urea does not interact directly with the proteins in the DLVO model. Instead, it alters the dielectric properties of the solvent, effectively modifying the solution environment. An increase in dielectric permittivity slightly reduces electrostatic interactions but more significantly lowers the Hamaker constant, which diminishes the strength of van der Waals attraction. Thus, salt and urea have opposing effects: salt reduces repulsion and thereby increases net attraction, while urea leaves electrostatic repulsion largely unchanged but weakens van der Waals attraction, leading to a net increase in repulsive interactions. Non-DLVO contributions, such as hydration, hydrogen bonding, or hydrophobic effects, are not treated explicitly but are effectively captured by a constant short-range cutoff in the b_2 calculation, independent of urea and salt concentrations. We note that, despite its simplicity, the DLVO model has also successfully captured the b_2 dependence on other factors, such as pH[94] and temperature,[95] as well as other additives, such as glycerol[96] and ethanol.[97]

Fig. 3a shows the behavior of the normalized second virial coefficient b_2 as a function of salt concentration for various urea concentrations. This data was calculated using parameters from earlier work.[60] For simplicity, the small temperature difference (solubility data at 18.9 °C *versus* b_2 model calculation at 20.0 °C) is neglected in this analysis, as previous work[95] has shown that such a minor change in temperature has a negligible effect on b_2, far smaller than the typical experimental uncertainty. We observe a decrease in the second virial coefficient with increasing salt concentration, as well as an increase with rising urea concentration at a fixed salt concentration. The fact that interactions become more attractive with the addition of salt and less attractive with the addition of urea is reflected in their effects on the state diagram (Fig. 1a).

These calculations allow us to quantify the interactions for each condition under which solubility was experimentally

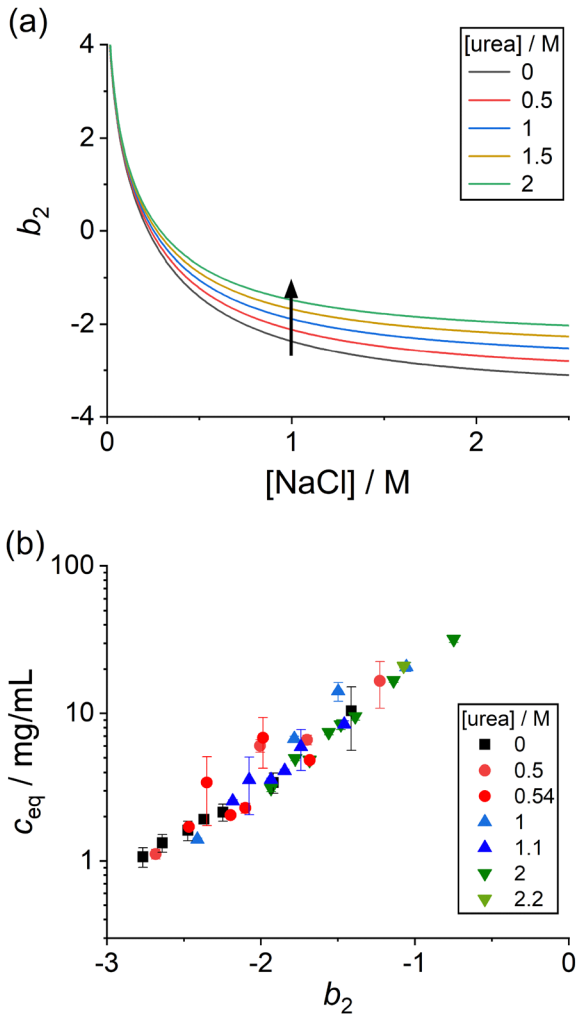

Fig. 3 Solubility and interactions. (a) Second virial coefficient normalized to the respective hard-sphere value (b_2) as a function of NaCl concentration for various urea concentrations (as indicated). The lines represent DLVO model calculations with parameters from ref. 60, in which quantitative agreement with experimental b_2 data was demonstrated. Increasing urea concentration is indicated by an arrow. (b) Solubility (c_{eq}) of tetragonal lysozyme crystals as a function of b_2 (instead of NaCl or urea concentration as in Fig. 2), including additional data.

determined. Fig. 3b shows the solubility (data from Fig. 2 as well as additional data) not as a function of urea or salt concentration, but as a function of the second virial coefficient instead. Remarkably, the data for different urea and salt concentrations collapse onto a single master curve in this plot. This collapse onto a single master curve suggests that protein–protein interactions, as quantified by the second virial coefficient, are a dominant factor in controlling solubility. This finding is consistent with the work by Guo *et al.*[78] and others,[98–100] which have proposed a correlation between the second virial coefficient and solubility. Here, this relationship is experimentally confirmed across a broad range of salt and urea concentrations. The observation that solubility data collapse onto a unified curve, regardless of whether salt or urea is varied, indicates that both additives affect solubility primarily through their impact on b_2, without significant cross-interactions. In line with this, salt and urea act through distinct physical mechanisms as described by the DLVO model: salt primarily screens electrostatic repulsion, whereas urea alters the dielectric constant of the medium, thereby modulating van der Waals attraction. While direct interactions between urea and protein surfaces cannot be ruled out, such effects are not explicitly included in the DLVO framework. Nevertheless, the DLVO-based model was shown to quantitatively describe the experimentally determined b_2 values across a wide range of salt and urea concentrations.[60] Taken together, these results suggest that solubility can be predicted by considering the independent contributions of salt and urea to protein–protein interactions, as reflected in the second virial coefficient.

It should be noted that the observed collapse of solubility data onto a single curve as a function of b_2 does not imply the absence or irrelevance of many-body interactions within the crystal. For example, the electrostatic neutrality of the crystal and counterion partitioning, as highlighted in ref. 92, remain important factors. Under our experimental conditions, however, such many-body effects appear to be either quantitatively minor or effectively incorporated into the parameters of the coarse-grained interaction model. Notably, the DLVO-based calculations yield values for b_2 that are in quantitative agreement with experimental measurements across the explored range of salt and urea concentrations.[60] Consequently, despite its simplifications, the DLVO-based b_2 serves as a reliable phenomenological parameter linking microscopic protein interactions to macroscopic solubility and crystallization behavior.

For completeness, we note that there have also been efforts to relate protein solubility in multicomponent solutions to preferential interaction parameters.[101,102] These parameters, in turn, influence the second virial coefficient through a protein–solvent interaction term.[103]

3.4. The driving force for crystallization

Crystallization is driven by the difference in chemical potential between the solute in solution and in the crystal, $\Delta\mu$.[104,105] Although often termed the "driving force" in the literature,[106] it is important to note that $\Delta\mu$ is a thermodynamic quantity with units of energy (specifically, molar Gibbs energy), not a mechanical force. Therefore, it may be more accurate to describe it as the driving energy for crystallization.[107,108] At equilibrium, $\Delta\mu = 0$, meaning the solute concentration in solution (c) equals the solubility concentration (c_{eq}). In general, $\Delta\mu$ can thus be expressed as:

$$\Delta\mu = (\mu^0 + kT\ln\gamma c) - (\mu^0 + kT\ln\gamma_{eq}c_{eq}), \quad (6)$$

where μ^0 is the standard-state chemical potential, c is the solute (protein) concentration, and γ is the thermodynamic activity coefficient of the solute.

The relationship between the interaction potential and $\Delta\mu$ is established through a virial expansion in protein concentration. The activity coefficient of the protein can be expressed

in terms of the virial coefficients:[109]

$$\ln \gamma = 2\frac{N_A}{M_w}B_2 c + \ldots, \quad (7)$$

where N_A is Avogadro's number and M_w is the molar mass of the protein, from which it follows that

$$\frac{\Delta\mu}{kT} = \ln\left(\frac{\gamma c}{\gamma_{eq} c_{eq}}\right) = \ln\left(\frac{c}{c_{eq}}\right) + 2\frac{N_A}{M_w}B_2(c - c_{eq}) + \ldots. \quad (8)$$

If the protein concentration is low or the attractive interactions are weak, only the ideal solution term remains:

$$\frac{\Delta\mu}{kT} \approx \ln\left(\frac{c}{c_{eq}}\right). \quad (9)$$

In this study, the protein concentration is held constant at a low value of c = 20 mg mL^{-1}. Based on the b_2 data presented in Fig. 3a, the leading non-ideal correction in eqn (8) is typically no more than 10% of the ideal-solution term (eqn (9)). This small correction is therefore neglected in our analysis.

Using this description of the chemical potential difference, along with the parameterization of the solubility data, we can calculate $\Delta\mu$ for all solution conditions. This allows us to create a map of $\Delta\mu$ for the state diagram (Fig. 1a). Based on the parameterization in eqn (1) and (2), $\Delta\mu$ is logarithmically dependent on sodium chloride concentration and linearly dependent on urea concentration. This is exemplified in Fig. 4a using the data from Fig. 2. In Fig. 4b, a mapping of $\Delta\mu$ is shown for the state diagram from Fig. 1a.

The crystallization boundary marks the region where protein crystals spontaneously form on experimental time scales. We observe that the crystallization boundary corresponds approximately to the condition where $\Delta\mu/kT \approx 1$. This is reasonable, as at this point, the driving force for crystallization exceeds the thermal energy. On the other hand, this implies that the solution must be supersaturated by a factor of almost 3, as also observed in previous studies.[21]

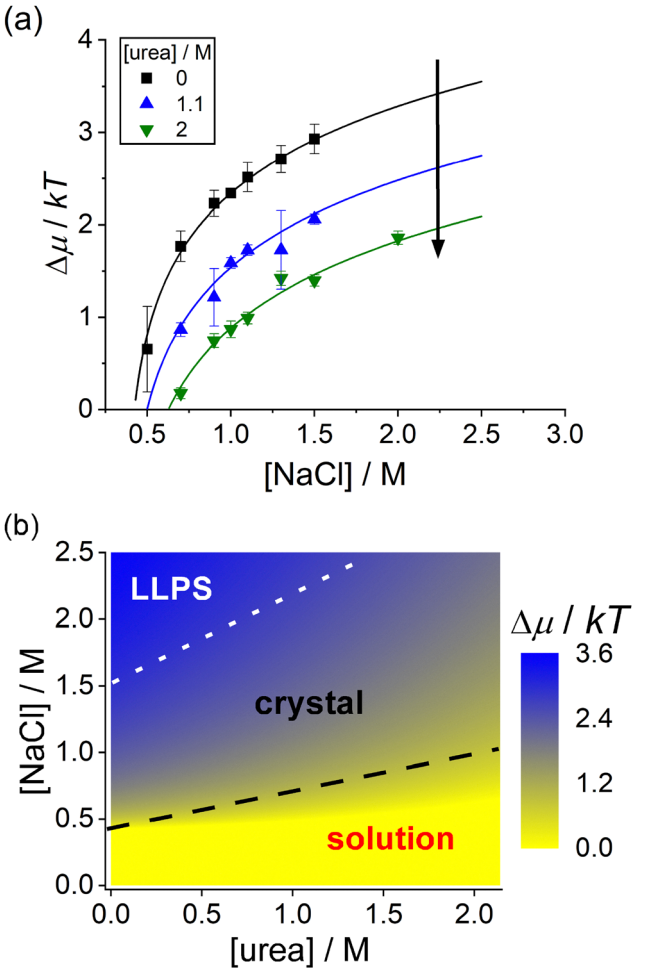

Fig. 4 Chemical potential difference as the driving force of crystallization. (a) Chemical potential difference ($\Delta\mu$), calculated from the solubility data in Fig. 2 according to eqn (9), as a function of NaCl concentration for various urea concentrations (as indicated): data (symbols) and lines (corresponding to the fits from Fig. 2 converted to $\Delta\mu$). Increasing urea concentration is indicated by an arrow. (b) Schematic state diagram in the urea–NaCl space from Fig. 1a, including a map of the chemical potential difference $\Delta\mu$ (as indicated).

3.5. Nucleation kinetics

Based on the state diagram (Fig. 1) and the extensive solubility data (Fig. 2), we now present an initial investigation of the effects of urea addition on crystallization kinetics. We focus on three different experimental series. First, we examine various salt concentrations as a reference without urea, which has already been studied in the literature. Second, we look at the impact of different salt concentrations at a fixed urea concentration of 2 M, the highest concentration used in the state diagram investigation (Fig. 1a). Finally, we study the effect of varying urea concentrations at a fixed salt concentration of 0.9 M, where tetragonal crystals form without kinetic roughening (Fig. 1b). We thus study how the simultaneous presence of urea and NaCl influences the crystallization kinetics. Additionally, using the solubility data (Fig. 2) and the chemical potential map (Fig. 4b), we can assess whether simple theoretical models, which typically consider kinetic parameters as a function of $\Delta\mu$, can be applied to describe the observed kinetics.

Focusing on the initially formed crystals, the bulk protein concentration is expected to be very close to the initial protein concentration, making the simple determination of $\Delta\mu$ with c = 20 mg mL^{-1} in eqn (9) valid. However, for crystals that form at later stages, this approach would be inaccurate, as the bulk concentration decreases during crystallization, which in turn affects $\Delta\mu$ according to eqn (9).

The crystallization induction time, t_{ind}, is a key parameter characterizing nucleation kinetics, as shown in Fig. 5 for varying urea and salt concentrations. Experimentally, t_{ind} comprises three contributions:[74] (1) the time required for the system to establish a metastable cluster size distribution, (2) the stochastic waiting time for the formation of the first critical nucleus (the nucleation time t_{nuc}), and (3) the subsequent growth time necessary for the nucleus to reach a detectable size.

While all three factors influence the measured induction time, classical nucleation theory (CNT) – discussed in more detail below – describes only the nucleation waiting time. CNT

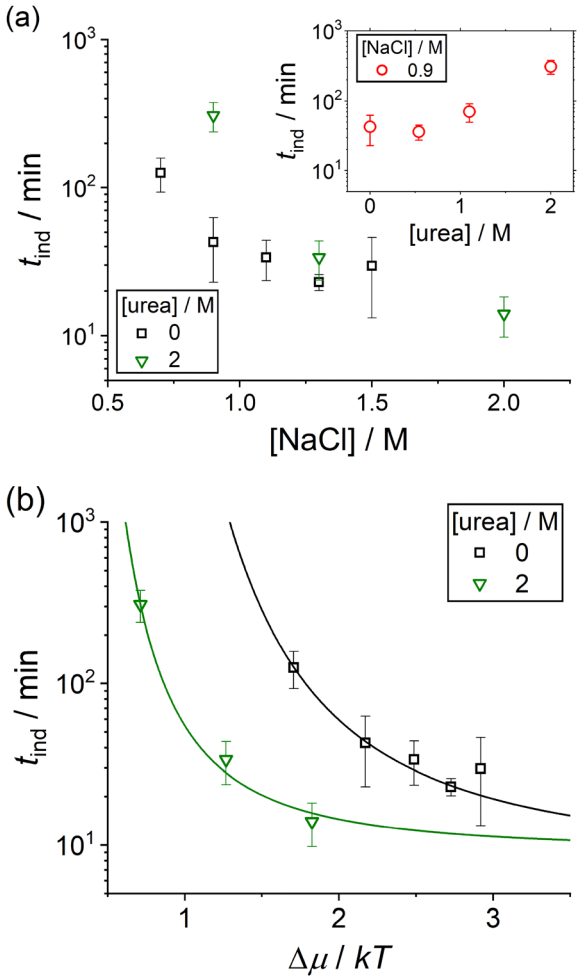

Fig. 5 Nucleation kinetics. (a) Crystallization induction times (t_{ind}) as a function of NaCl concentration with and without 2 M urea (as indicated). (inset) Crystallization induction times (t_{ind}) as a function of urea concentration at 0.9 M NaCl. (b) Crystallization induction times (t_{ind}) shown in (a), but now plotted as a function of the chemical potential difference $\Delta\mu$ instead of NaCl concentration. Lines are fits to the CNT model according to eqn (10)–(12).

relates the nucleation rate J, defined as the number density of new stable nuclei formed per unit time and volume, and nucleation time *via* $VJ\langle t_{nuc}\rangle = 1$, where V is the experimental volume and $\langle\cdot\rangle$ denotes the expectation value. This relation follows directly from the Poisson statistics of nucleation events, where the probability of no nucleus forming before time t is $P(t) = \exp(-VJt)$.[110,111]

Given that only the total induction time t_{ind} is experimentally measurable, we assume – supported by previous work on lysozyme in brine[75] – that both the relaxation time (1) and the growth time (3) are small compared to the nucleation time (2) and approximately constant under our controlled experimental conditions. This assumption allows the approximation

$$t_{ind} \approx t_{nuc} \propto J^{-1}, \quad (10)$$

facilitating a direct comparison of CNT predictions with the measured induction times.

In Fig. 5a, at a fixed urea concentration, the induction time decreases with increasing NaCl concentration. However, for the dataset without urea, the induction time appears to increase again at the highest NaCl concentration. The inset in Fig. 5a shows that at a fixed salt concentration of 0.9 M NaCl, the induction time increases with higher urea concentrations. Similar to the effects observed on the state diagram and interactions, NaCl and urea have opposing influences on induction time.

The decrease in induction time upon salt addition can be interpreted as follows: at low salt concentrations, strong electrostatic repulsion between proteins inhibits aggregation and crystal formation. When salt is added, it screens these repulsive forces, allowing proteins to approach each other more easily. This reduction in repulsion promotes faster aggregation, as proteins are more likely to nucleate. Additionally, salt can enhance specific interactions between proteins, such as hydrophobic interactions, further accelerating nucleation and crystallization, though these short-range effects are not explicitly considered in the DLVO model used in Section 3.3.

The apparent non-monotonic behavior of induction times for the NaCl-only data suggests that the highest NaCl concentration was measured near the LLPS state boundary (see Fig. 1a). A previous study observed that the nucleation rate exhibits a maximum near the LLPS state boundary,[112] and the observed minimum in induction times here aligns with this result.

The observed increase in induction time upon urea addition can be rationalized as follows: in salt-rich environments, where electrostatic repulsion is strongly screened, proteins tend to associate rapidly, often leading to nonspecific aggregation. By moderating interactions and slowing down aggregation kinetics, urea allows proteins to sample a broader range of configurations, which increases the likelihood of forming ordered nuclei rather than amorphous aggregates. As a result, urea extends the induction time but ultimately promotes more controlled and productive crystallization. These considerations are revisited and generalized in Section 3.7.

In Fig. 5b, the induction times from Fig. 5a are plotted as a function of $\Delta\mu$, according to the calculation shown in Fig. 4b. For the datasets without urea and with 2 M urea, induction times decrease progressively with increasing $\Delta\mu$. Additionally, it is notable that at a fixed $\Delta\mu$, the curve in the presence of 2 M urea is shifted toward lower induction times. This suggests that the conditions for lysozyme crystal nucleation could be optimized exploiting the systematic solubility data provided here.

Although recent research has focused on non-classical nucleation mechanisms in protein solutions, particularly two-step processes,[113–116] here we use classical nucleation theory (CNT),[74] likely the simplest and most widely known theory of nucleation, in order to describe the dependence of the nucleation rate on $\Delta\mu$. Nucleation in CNT is the formation of a critical nucleus that transitions from a metastable state in a supersaturated solution to a stable phase. This process involves a balance between the favorable enthalpy change from cluster growth and the unfavorable surface energy from new interfaces. The nucleus must reach a critical size to become stable enough

for growth. Nucleation is a thermally activated process, requiring the overcoming of an energy barrier that arises from this balance. The rate of nucleation J depends on the thermal energy available to surmount this barrier:

$$J = A\exp\left(-\frac{\Delta G^*}{kT}\right), \quad (11)$$

where A is a pre-exponential kinetic factor and ΔG^* is the thermodynamic nucleation barrier, given by:

$$\Delta G^* = \frac{16}{3}\pi {v_0}^2 \frac{\gamma^3}{(\Delta\mu)^2} \quad (12)$$

here, v_0 is the volume of a protein in the crystal (assumed to be v_0 = 30 nm^3),[27] and γ is the crystal-solution interfacial free energy.[117] The factor A accounts for the frequency of attempts to form the nucleus, which is related to the diffusion coefficient of the molecules in the solution and the size of the critical nucleus. However, based on measurements of t_{ind}, accurately estimating A is challenging, as eqn (10) is only an approximation and does not account for the equilibration time or the time required for the crystal to grow large enough to be detectable.

Using eqn (10)–(12), the data in Fig. 5b can be described (solid lines), yielding:

$$\gamma = 0.9\frac{kT}{\sigma^2} \quad (\text{only NaCl}),$$

$$\gamma = 0.6\frac{kT}{\sigma^2} \quad (2\,\text{M urea}).$$

Here, σ = 3.4 nm is the typical diameter of a lysozyme molecule. Our values for γ are similar to the value for a hard-sphere system (0.6 kT/σ^2, see ref. 118 and 119) and to those previously reported in the literature for lysozyme (1.2 kT/σ^2 in ref. 117 and 1.4–1.8 kT/σ^2 in ref. 27 and 63). The fit results for γ and eqn (12) suggest that adding urea may lower the nucleation barrier.

Modeling the nucleation rate J as a function of the chemical potential difference $\Delta\mu$ within classical nucleation theory (CNT) yields predictions consistent with our experimental data (Fig. 5b). This agreement supports the interpretation of the induction time t_{ind} as a kinetic parameter primarily governed by nucleation kinetics. While the relaxation and growth times were not directly measured, previous studies on similar systems suggest that these contributions are small.[75] The close correspondence between the CNT predictions and our measured induction times is therefore consistent with the assumption that relaxation and growth times contribute only marginally under our experimental conditions, justifying the approximation $t_{ind} \approx t_{nuc}$.

It is remarkable that even in such a complex system, the experimental data can be well described using the CNT model. The agreement between CNT and the experimental data indicates that the underlying nucleation barrier and thermodynamic parameters, such as $\Delta\mu$, play a crucial role in controlling the nucleation kinetics of crystallization. The fact that $\Delta\mu$ is modified by variations in the solution conditions shows that different environmental factors, such as salt and urea concentrations, significantly influence crystallization. These parameters can modify protein–protein interactions, affecting $\Delta\mu$ and, consequently, the nucleation process.

It is highly likely that nucleation in our system is heterogeneous,[120] meaning that the glass walls of the microscopy cell and possibly residual foreign particles that could not be filtered out from the solution influence the nucleation rate. However, even in this case, the functional form of the CNT model can still be applied, provided that the parameters are interpreted as effective parameters for heterogeneous nucleation. Specifically, the same functional dependence of the nucleation barrier on $\Delta\mu$ can be assumed.

It is important to note, though, that while the data are consistently described by CNT, they represent only a first step toward a more comprehensive analysis. The pre-exponential factor A and the interfacial energy γ in CNT could, in principle, depend on the solution conditions, such as the NaCl concentration. However, the assumption here is that the main influence on nucleation kinetics is determined by urea concentration, with the influence of NaCl expected to be small. This assumption is plausible, as it is supported by the consistency of the model with the data as well as the reasonable agreement of the value for γ with the literature. Moreover, in a previous study[121] involving protein solutions containing only NaCl, it was observed that solution conditions leading to equal solubility also resulted in equal nucleation rates and, consequently, identical kinetic parameters. This finding fully supports our assumption. Nevertheless, more extensive measurements, systematically varying $\Delta\mu$ by changing the protein concentration, could reveal a dependence of A and γ on NaCl concentration. Based on the previous observations, however, it is not expected that this effect would be significant.

3.6. Growth kinetics

In Fig. 6a, the results of growth rate G measurements for the (110) and (101) faces of tetragonal lysozyme crystals are shown, with urea concentrations (0 M and 2 M) as a function of NaCl concentration. The inset shows the data for a fixed NaCl concentration of 0.9 M as a function of urea concentration. At low salt concentrations, $G_{101} > G_{110}$, but at higher salt concentrations, this trend reverses. Both G_{110} and G_{101} increase with NaCl concentration, both in the presence and absence of urea. However, in the absence of urea, the increase becomes negligible at higher NaCl concentrations, with the highest data point even showing a decrease. Similarly, it was previously observed[122] that at high supersaturations, which may arise from elevated salt concentrations, the growth rates reach a maximum before beginning to decrease. The addition of urea results in a progressive decrease in both G_{110} and G_{101}. Without urea, $G_{110} > G_{101}$, but with increasing urea concentration, G_{101} surpasses G_{110}, and the difference grows with higher urea concentrations.

These observations of the growth rates confirm the conclusions drawn from the final morphology of lysozyme crystals (as shown in Fig. 1b), where differences in crystal shape were attributed to variations in G_{110}/G_{101}. The fact that growth rates in the absence of urea show only a slight increase or even a decrease at high NaCl concentrations correlates with the

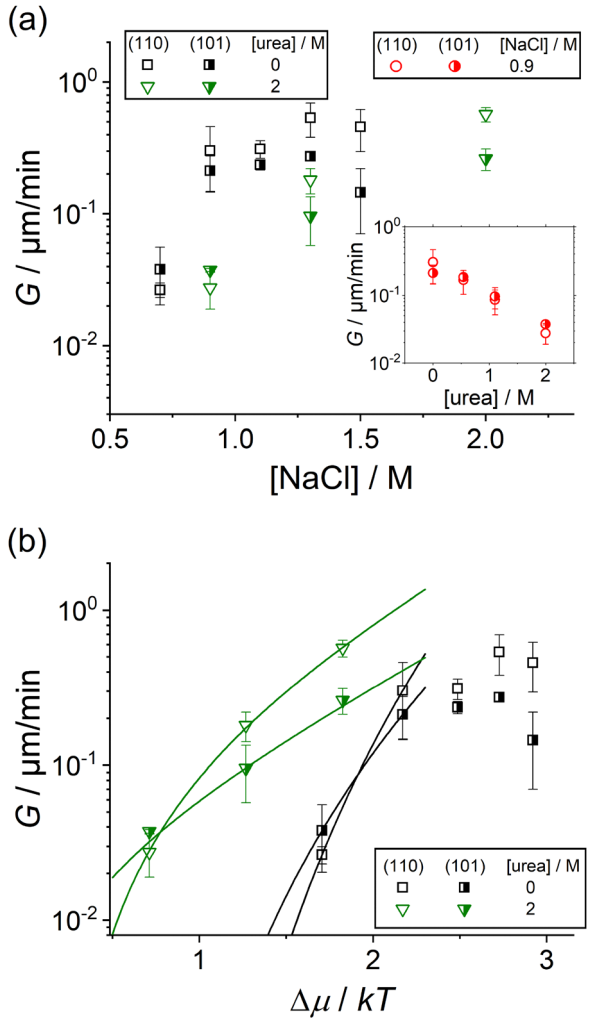

Fig. 6 Growth kinetics. (a) Crystal growth rates (G) of the (110) and (101) faces of tetragonal lysozyme crystals as a function of NaCl concentration with and without 2 M urea (as indicated). (inset) Crystal growth rates (G) of the (110) and (101) faces of tetragonal lysozyme crystals as a function of urea concentration with 0.9 M NaCl (as indicated). (b) Crystal growth rates (G) of the (110) and (101) faces of tetragonal lysozyme crystals, shown in (a), but now as a function of the chemical potential difference $\Delta\mu$ instead of NaCl concentration: data (symbols, as indicated) and fits to the 2D growth model (lines) according to eqn (13) (see text for details).

rounded or roughened crystal shape observed at such high NaCl concentrations.

Fig. 6b replots the data from Fig. 6a as a function of the chemical potential difference $\Delta\mu$ instead of NaCl concentration. At low to moderate $\Delta\mu$, the growth rate rises steeply with increasing $\Delta\mu$. However, beyond a certain point, the increase slows and eventually saturates or even declines, as observed in the absence of urea. This qualitative change signals a transition to a different growth regime, consistent with previous reports on lysozyme crystals grown in NaCl solutions.[123–126] Therefore, for moderate $\Delta\mu$ values – corresponding to sufficiently low salt concentrations – the data can be well described by a simple growth model, as outlined below.

In the "birth and spread" model of crystal growth, the crystal surface expands through two distinct processes: the birth of a new growth unit (layer) and the subsequent spreading of that layer as it incorporates more growth units. The "birth" refers to the formation of new layers, which can occur through the nucleation of 2D islands on the crystal surface. Once a new layer is formed, the "spread" process involves the incorporation of additional growth units at the step edges or kinks, allowing the layer to expand. For the formation of 2D nucleates on a smooth surface, the growth rate normal to the crystal surface is given by the following equation:[127]

$$G = \tilde{A}\left(\frac{\Delta\mu}{kT}\right)^{1/6}\exp\left(\frac{2\Delta\mu}{3kT}\right)\left[\exp\left(\frac{\Delta\mu}{kT}\right)-1\right]^{2/3} \times \exp\left(-\frac{\pi}{3}\left(\frac{\tilde{\gamma}}{kT}\right)^{2}\left(\frac{\Delta\mu}{kT}\right)^{-1}\right) \quad (13)$$

where $\tilde{\gamma}$ is the effective growth barrier. Again, the prefactor $\tilde{A}$ is related to the attempt frequency, which represents the rate at which the growth unit attempts to overcome the barrier. The effective barrier $\tilde{\gamma}$ can be related to the surface free energy of a step α *via* $\tilde{\gamma} = \alpha\sqrt{hv_0}$, where h is the step height.[123,124]

For the two data points without urea, we obtain $\tilde{\gamma} = 3.6kT$ for the (110) face and $\tilde{\gamma} = 2.7kT$ for the (101) face. These values are consistent with those previously reported for similar solution conditions.[123] Extensive measurements of the dependence of G on $\Delta\mu$ yielded the following results: $\tilde{\gamma} = (3.2 \pm 0.7)kT$ for the (110) face[125] and $\tilde{\gamma} = (2.4 \pm 0.5)kT$ for the (101) face.[126] Although only two data points were available for the model description in our dataset without urea (which is certainly insufficient to draw valid conclusions), it is worth noting that the results from the fitting procedure match with the literature values. This at least supports the validity of the presented results when compared to the literature.

The data points used for fitting were deliberately selected from the known applicability range of the simple growth model, that is moderate supersaturation ($\Delta\mu$) where the model reliably captures growth kinetics. Data at higher $\Delta\mu$ were excluded from the fit due to qualitative deviations in growth behavior. While the exact range of applicability depends on crystal face and solution conditions, this selection follows previous studies reporting deviations at higher supersaturation.[125,126]

For 2 M urea, this model was also applicable. Although both the (110) and (101) faces have a similarly limited dataset of only three data points each, the fit for the (110) face was more stable, yielding $\tilde{\gamma} = 1.1\ kT$. In contrast, fitting the growth of the (101) face proved more challenging due to data variability and limited data points. Consequently, no robust fit could be achieved; instead, a representative curve with $\tilde{\gamma} = 0.2\ kT$ is shown.

The data without urea at high salt concentrations could not be described by the simple growth model, as their dependence on $\Delta\mu$ could not be captured by the model. Literature suggests that data under such conditions can be described using a continuous growth model.[126] In another model, this observation, where crystals might crystallize too quickly in incorrect orientations, was accounted for by incorporating such non-productive configurations into a 2D growth model.[59] In the

presence of urea, the same value of G is reached at a significantly lower $\Delta\mu$ compared to the absence of urea (Fig. 6b). This observation could also be explained by the Schmit-Dill model[59] accounting for non-productive configurations, which suggests that the addition of a denaturant may accelerate crystal growth by destabilizing non-productive proteins.

As with the induction time measurements, the limitations discussed earlier also apply to these first growth rate measurements.

3.7. A general scenario for globular protein crystallization in the presence of nonspecific additives and salt

The results of the present work on the formation of tetragonal lysozyme crystals in the presence of urea and salt may have broader implications for globular protein crystallization in general. While these findings are based on a model protein, lysozyme, the arguments presented here are likely applicable to other globular proteins, provided that the non-electrostatic attractive interactions between protein molecules are sufficiently strong for crystallization. The scenario is illustrated in Fig. 7.

In the case of proteins at pH values close to their isoelectric point (pI), where the net charge is very small, electrostatic repulsions are weak and attractive forces dominate. This results in colloidal instability, favoring amorphous aggregation rather than the formation of regular crystal lattices (see Fig. 7a). Consequently, crystallization is often conducted at pH values further away from the pI, where proteins carry a significant net charge (see Fig. 7b).

At these conditions, additional ions are necessary to screen the increased electrostatic repulsions due to the greater net charge. These ions also need to be incorporated into the crystal and its unit cell, since the macroscopic crystal is expected to be electrostatically neutral, and it follows that the elementary cell is also neutral. Thus, ions must be sequestered together with proteins during crystal formation. The crystal itself is likely stabilized by non-electrostatic attractive interactions, including van der Waals forces, hydrogen bonding, and hydrophobic effects. However, the addition of salt reduces electrostatic repulsions, and at high salt concentrations, while required for maintaining charge neutrality of the crystal, the reduction in repulsion can lower the energy barrier for aggregation, favoring amorphous aggregation over crystallization (see Fig. 7c).

In this context, the addition of urea can be beneficial. Urea lowers nonspecific attractions,[60] enabling a delicate balance: sufficient ions are incorporated into the crystal to maintain charge neutrality, but the excessive reduction in repulsion is mitigated, helping to avoid the formation of amorphous aggregates. Thus, urea can facilitate the identification of an optimal crystallization environment, where electrostatic screening and favorable nonspecific interactions converge, improving the chances of crystallization (see Fig. 7d). Other nonspecific additives, such as glycerol or ethanol, might serve a similar purpose, further lowering attractions and helping to optimize the crystallization process.

Like urea, these additives have been experimentally shown to lower the LLPS coexistence temperature and increase the

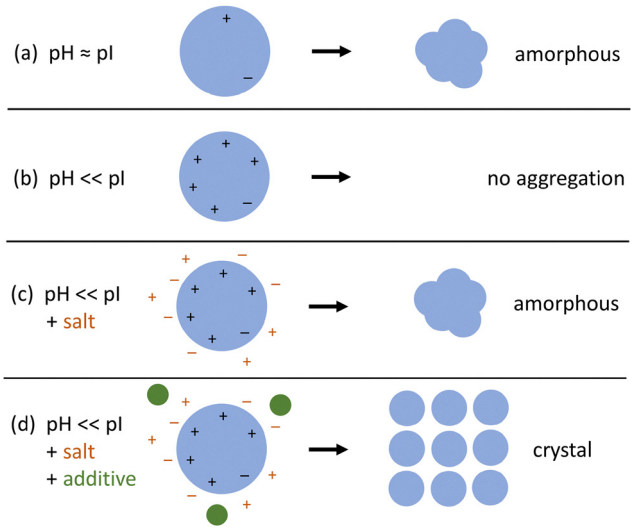

Fig. 7 Schematic illustration of the scenario for globular protein crystallization in the presence of salts and nonspecific additives. (a) When the pH of the solution is near the isoelectric point (pI), the protein (represented as a large blue sphere) carries few charges. As a result, the attractive interactions between proteins are not shielded, leading to easy aggregation into amorphous clusters (depicted schematically as an unordered lump; for clarity, individual protein molecules are shown at reduced size and without charges). (b) When the pH is far from the pI, the protein carries a net positive charge, making repulsive interactions dominant and hindering aggregation. (c) In the presence of salt ions (depicted as red positive and negative signs around the protein), these ions shield the protein charges, reducing the impact of the repulsive interactions. This favors the formation of amorphous aggregates. (d) When, in addition to the conditions in (c), nonspecific additives such as urea (illustrated as small green spheres around the protein) are introduced, the situation changes. Urea slightly reduces the attractive forces between proteins, preventing the formation of amorphous aggregates caused by excessive attraction, and promoting crystallization (illustrated as a regularly ordered protein structure).

second virial coefficient b_2, indicating an overall reduction in net attractive interactions between protein molecules.[16,97] Additionally, their presence raises the dielectric constant of the solution. Within the framework of a simplified DLVO model,[60] this increase modulates both electrostatic and van der Waals interactions, resulting in a weakening of attractive forces accompanied by a slight decrease in repulsive interactions. Although this model neglects the complexity of specific binding sites and directional interactions inherent to proteins, it quantitatively captures the effect of these additives on b_2, providing a consistent and predictive physicochemical rationale for how nonspecific additives influence intermolecular interactions and phase behavior in protein solutions.

The effects of salt and urea on protein crystallization are also reflected in their influence on solubility, nucleation, and growth. Salt, by screening electrostatic repulsions, decreases protein solubility, which can facilitate nucleation and crystal growth. However, at very high salt concentrations, the energy barrier for amorphous aggregation may become too low, potentially inhibiting proper crystallization. Urea, in contrast, increases protein solubility by weakening attractive interactions, thereby typically reducing both nucleation rates and growth. Nonetheless, at

non-denaturing concentrations, urea may shift the balance in favor of nucleation without promoting aggregation, resulting in more controlled crystal growth. By modulating solubility and intermolecular interactions through these additives, a fine-tuned environment for optimal protein crystallization can be achieved.

4. Conclusion

In conclusion, this study provides a detailed analysis of how urea and salt modulate the crystallization of lysozyme by affecting both thermodynamic and kinetic parameters. Urea increases protein solubility at sub-denaturing concentrations by weakening attractive interactions, while sodium chloride decreases solubility by screening electrostatic repulsions, without inducing a salting-in effect. Quantifying protein–protein interactions *via* the second virial coefficient (B_2) reveals that solubility data collapse onto a master curve when plotted against B_2, underlining the dominant role of interparticle interactions. Furthermore, the chemical potential difference ($\Delta\mu$) increases logarithmically with salt concentration and decreases linearly with urea concentration, providing a direct thermodynamic link to crystallization driving forces.

Crystallization kinetics monitored by video microscopy show that salt shortens induction times and accelerates crystal growth, while urea generally slows these processes. Notably, when compared at a fixed $\Delta\mu$, urea facilitates both nucleation and growth, enabling crystallization already at lower supersaturation levels. These observations are well captured by classical nucleation theory and a birth-and-spread growth model.

Overall, our results demonstrate that salt and urea independently modulate protein–protein interactions and crystallization behavior. This suggests a general strategy: by fine-tuning solution conditions using salts and nonspecific additives like urea, it is possible to optimize the delicate balance between attractive and repulsive forces required for successful protein crystallization. Beyond lysozyme, this approach could be extended to a wide range of globular proteins, offering new opportunities for rational crystallization design in structural biology, pharmaceutical development, and biomaterials research.

Author contributions

T. H. performed the experiments and analyzed the data. F. P. conceived and supervised the project, led the data analysis, wrote the manuscript, and secured funding. Both authors reviewed and approved the final manuscript.

Conflicts of interest

There are no conflicts to declare.

Data availability

The data that support the findings of this study are available within the article.

Acknowledgements

We are grateful to Stefan U. Egelhaaf (Düsseldorf) for inspiring discussions and his continuous support. We deeply mourn his untimely passing. We also thank Jan K. G. Dhont (Jülich) for very valuable discussions and thoughtful comments. Financial support by the German Research Foundation (DFG Grant No. 495795796) is gratefully acknowledged.

Notes and references

1 J. J. McManus, P. Charbonneau, E. Zaccarelli and N. Asherie, *Curr. Opin. Colloid Interface Sci.*, 2016, **22**, 73–79.
2 A. Stradner and P. Schurtenberger, *Soft Matter*, 2020, **16**, 307–323.
3 R. Mezzenga and P. Fischer, *Rep. Prog. Phys.*, 2013, **76**, 046601.
4 J. D. Gunton, A. Shiryayev and D. L. Pagan, *Protein condensation, Kinetic pathways to crystallization and disease*, Cambridge University Press, 2007.
5 P. G. Vekilov, *Soft Matter*, 2010, **6**, 5254–5272.
6 W. Wang, *Int. J. Pharm.*, 2005, **289**, 1–30.
7 Y. Shen, A. Levin, A. Kamada, Z. Toprakcioglu, M. Rodriguez-Garcia, Y. Xu and T. P. J. Knowles, *ACS Nano*, 2021, **15**, 5819–5837.
8 L. R. De Young, A. L. Fink and K. A. Dill, *Acc. Chem. Res.*, 1993, **26**, 614–620.
9 A. McPherson, *Methods*, 2004, **34**, 254–265.
10 D. Fusco and P. Charbonneau, *Colloids Surf. B*, 2016, **137**, 22–31.
11 F. Chiti and C. M. Dobson, *Ann. Rev. Biochem.*, 2006, **75**, 333–366.
12 A. K. Buell, C. M. Dobson and T. P. Knowles, *Essays Biochem.*, 2014, **56**, 11–39.
13 A. A. Hyman, C. A. Weber and F. Jülicher, *Annu. Rev. Cell Dev. Biol.*, 2014, **30**, 39–58.
14 D. Shukla, C. P. Schneider and B. L. Trout, *Adv. Drug. Delivery Rev.*, 2011, **63**, 1074–1085.
15 F. Zhang, F. Roosen-Runge, A. Sauter, M. Wolf, R. M. J. Jacobs and F. Schreiber, *Pure Appl. Chem.*, 2014, **86**, 191–202.
16 J. Hansen, F. Platten, D. Wagner and S. U. Egelhaaf, *Phys. Chem. Chem. Phys.*, 2016, **18**, 10270–10280.
17 B. Smejkal, B. Helk, J.-M. Rondeau, S. Anton, A. Wilke, P. Scheyerer, J. Fries, D. Hekmat and D. Weuster-Botz, *Biotechnol. Bioeng.*, 2013, **110**, 1956–1963.
18 J. Ferreira, J. Opsteyn, F. Rocha, F. Castro and S. Kuhn, *Chem. Eng. Res. Des.*, 2020, **162**, 249–257.
19 K. Kang and F. Platten, *Sci. Rep.*, 2022, **12**, 3061.
20 D. Ray, M. Madani, J. K. G. Dhont, F. Platten and K. Kang, *Soft Matter*, 2025, **21**, 3012–3021.
21 S. D. Durbin and G. Feher, *Annu. Rev. Phys. Chem.*, 1996, **47**, 171–204.
22 P. G. Vekilov and A. A. Chernov, *Solid State Phys.*, 2003, **57**, 1–147.

23 A. McPherson and J. A. Gavira, *Acta Crystallogr., Sect. F: Struct. Biol. Cryst. Commun.*, 2014, **F70**, 2–20.
24 J. Ferreira and F. Castro, *CrystEngComm*, 2023, **25**, 6388–6404.
25 S. R. Trevino, J. Scholtz and C. Pace, *J. Pharm. Sci.*, 2008, **97**, 4155–4166.
26 S. Whitelam and R. L. Jack, *Annu. Rev. Phys. Chem.*, 2015, **66**, 143–163.
27 O. Galkin and P. G. Vekilov, *J. Phys. Chem. B*, 1999, **103**, 10965–10971.
28 C. N. Nanev, F. V. Hodzhaoglu and I. L. Dimitrov, *Cryst. Growth Des.*, 2011, **11**, 196–202.
29 C. N. Nanev, *Prog. Cryst. Growth Charact. Mater.*, 2013, **59**, 133–169.
30 C. N. Nanev, *J. Cryst. Growth*, 2023, **607**, 127101.
31 J. Wiencek, *Annu. Rev. Biomed. Eng.*, 1999, **1**, 505–534.
32 R. P. Sear, *J. Phys.: Condens. Matter*, 2007, **19**, 033101.
33 F. Zhang, *J. Phys.: Condens. Matter*, 2017, **29**, 443002.
34 M. Sleutel and A. E. S. Van Driessche, *Nanoscale*, 2018, **10**, 12256–12267.
35 D. Bolen, *Methods*, 2004, **34**, 312–322.
36 P. G. Vekilov, *Cryst. Growth Des.*, 2007, **7**, 2239–2246.
37 H. Hamada, T. Arakawa and K. Shiraki, *Curr. Pharm. Biotechnol.*, 2009, **10**, 400–407.
38 S. Tanaka and M. Ataka, *J. Chem. Phys.*, 2002, **117**, 3504–3510.
39 M. D. Senft, G. Zocher, S. Retzbach, R. Maier, A. Hiremath, F. Zhang, T. Stehle and F. Schreiber, *Cryst. Growth Des.*, 2025, **25**, 2418–2429.
40 J. J. McManus, A. Lomakin, O. Ogun, A. Pande, M. Basan, J. Pande and G. B. Benedek, *Proc. Natl. Acad. Sci. U. S. A.*, 2007, **104**, 16856–16861.
41 M. K. Quinn, S. James and J. J. McManus, *J. Phys. Chem. B*, 2019, **123**, 4373–4379.
42 J. Berthou and P. Jollès, *FEBS Lett.*, 1973, **31**, 189–192.
43 Y. Nozaki and C. Tanford, *J. Biol. Chem.*, 1963, **238**, 4074–4081.
44 C. Pace, *Methods Enzymol.*, 1986, **131**, 266–280.
45 G. I. Makhatadze and P. L. Privalov, *J. Mol. Biol.*, 1992, **226**, 491–505.
46 A. Soper, E. Castner and A. Luzar, *Biophys. Chem.*, 2003, **105**, 649–666.
47 D. Tobi, R. Elber and D. Thirumalai, *Biopolymers*, 2003, **68**, 359–369.
48 S. N. Timasheff and G. Xie, *Biophys. Chem.*, 2003, **105**, 421–448.
49 L. Hua, R. Zhou, D. Thirumalai and B. J. Berne, *Proc. Natl. Acad. Sci. U. S. A.*, 2008, **105**, 16928–16933.
50 B. J. Bennion and V. Daggett, *Proc. Natl. Acad. Sci. U. S. A.*, 2003, **100**, 5142–5147.
51 L. B. Sagle, Y. Zhang, V. A. Litosh, X. Chen, Y. Cho and P. S. Cremer, *J. Am. Chem. Soc.*, 2009, **131**, 9304–9310.
52 D. R. Canchi, D. Paschek and A. E. García, *J. Am. Chem. Soc.*, 2010, **132**, 2338–2344.
53 D. R. Canchi and A. E. García, *Ann. Rev. Phys. Chem.*, 2013, **64**, 273–293.
54 Z. Su and C. L. Dias, *J. Mol. Liquids*, 2017, **228**, 168–175.
55 D. Niether, S. Di Lecce, F. Bresme and S. Wiegand, *Phys. Chem. Chem. Phys.*, 2018, **20**, 1012–1020.
56 A. K. Hüsecken, F. Evers, C. Czeslik and M. Tolan, *Langmuir*, 2010, **26**, 13429–13435.
57 F. Evers, R. Steitz, M. Tolan and C. Czeslik, *Langmuir*, 2011, **27**, 6995–7001.
58 K. Kitamura, A. Oshima, F. Sasaki, Y. Shiramasa, R. Yamamoto, T. Kameda, S. Kitazawa and R. Kitahara, *J. Phys. Chem. Lett.*, 2024, **15**, 7620–7627.
59 J. D. Schmit and K. Dill, *J. Am. Chem. Soc.*, 2012, **134**, 3934–3937.
60 M. Madani, T. Hamacher and F. Platten, *Soft Matter*, 2025, **21**, 1937–1948.
61 F. Platten, J. Hansen, J. Milius, D. Wagner and S. U. Egelhaaf, *J. Phys. Chem. B*, 2015, **119**, 14986–14993.
62 J. R. Warren and J. A. Gordon, *J. Phys. Chem.*, 1966, **70**, 297–300.
63 A. M. Kulkarni and C. F. Zukoski, *Langmuir*, 2002, **18**, 3090–3099.
64 E. L. Forsythe, R. A. Judge and M. L. Pusey, *J. Chem. Eng. Data*, 1999, **44**, 637–640.
65 Y. Liu, X. Wang and C. B. Ching, *Cryst. Growth Des.*, 2010, **10**, 548–558.
66 V. Bhamidi, S. Varanasi and C. A. Schall, *Cryst. Growth Des.*, 2002, **2**, 395–400.
67 F.-X. Schmid, in *Biological Macromolecules: UV-visible Spectrophotometry*, John Wiley & Sons, Ltd, 2001.
68 A. F. Ducruix and M. M. Ries-Kautt, *Methods*, 1990, **1**, 25–30.
69 N. Asherie, *Methods*, 2004, **34**, 266–272.
70 G. Feher and Z. Kam, *Methods Enzymol.*, 1985, **114**, 77–112.
71 M. Ataka and M. Asai, *J. Cryst. Growth*, 1988, **90**, 86–93.
72 M. Ataka and M. Asai, *Biophys. J.*, 1990, **58**, 807–811.
73 D. Ray, M. Madani, J. K. G. Dhont, F. Platten and K. Kang, *J. Phys. Chem. Lett.*, 2024, **15**, 8108–8113.
74 J. W. Mullin, *Crystallization*, Butterworth-Heinemann, Oxford, 2001.
75 L. Goh, K. Chen, V. Bhamidi, G. He, N. C. S. Kee, P. J. A. Kenis, C. F. I. Zukoski and R. D. Braatz, *Cryst. Growth Des.*, 2010, **10**, 2515–2521.
76 M. C. R. Heijna, W. J. P. v Enckevort and E. Vlieg, *Cryst. Growth Des.*, 2008, **8**, 270–274.
77 S. Durbin and G. Feher, *J. Cryst. Growth*, 1986, **76**, 583–592.
78 B. Guo, S. Kao, H. McDonald, A. Asanov, L. Combs and W. W. Wilson, *J. Cryst. Growth*, 1999, **196**, 424–433.
79 G. A. Vliegenthart and H. N. W. Lekkerkerker, *J. Chem. Phys.*, 2000, **112**, 5364–5369.
80 F. Zhang, F. Roosen-Runge, M. W. A. Skoda, R. M. J. Jacobs, M. Wolf, P. Callow, H. Frielinghaus, V. Pipich, S. Prevost and F. Schreiber, *Phys. Chem. Chem. Phys.*, 2012, **14**, 2483–2493.
81 J. Hansen, J. N. Pedersen, J. S. Pedersen, S. U. Egelhaaf and F. Platten, *J. Chem. Phys.*, 2022, **156**, 244903.
82 S. Gorti, J. Konnert, E. L. Forsythe and M. L. Pusey, *Cryst. Growth Des.*, 2005, **5**, 535–545.

83 S. B. Howard, P. J. Twigg, J. K. Baird and E. J. Meehan, *J. Cryst. Growth*, 1988, **90**, 94–104.
84 M. M. Ries-Kautt and A. F. Ducruix, *J. Biol. Chem.*, 1989, **264**, 745–748.
85 E. Cacioppo and M. L. Pusey, *J. Cryst. Growth*, 1991, **114**, 286–292.
86 J.-P. Guilloteau, M. M. Riès-Kautt and A. F. Ducruix, *J. Crys. Growth*, 1992, **122**, 223–230.
87 E. J. Cohn, *Physiol. Rev.*, 1925, **5**, 349–437.
88 A. A. Green, *J. Biol. Chem.*, 1931, **93**, 495–516.
89 A. A. Green, *J. Biol. Chem.*, 1932, **95**, 47–66.
90 P. Retailleau, M. Riès-Kautt and A. Ducruix, *Biophys. J.*, 1997, **73**, 2156–2163.
91 W. Melander and C. Horváth, *Arch. Biochem. Biophys.*, 1977, **183**, 200–215.
92 J. D. Schmit and K. A. Dill, *J. Phys. Chem. B*, 2010, **114**, 4020–4027.
93 L. Hentschel, J. Hansen, S. U. Egelhaaf and F. Platten, *Phys. Chem. Chem. Phys.*, 2021, **23**, 2686–2696.
94 F. Platten, N. E. Valadez-Pérez, R. Castañeda Priego and S. U. Egelhaaf, *J. Chem. Phys.*, 2015, **142**, 174905.
95 F. Platten, J. Hansen, J. Milius, D. Wagner and S. U. Egelhaaf, *J. Phys. Chem. Lett.*, 2016, **7**, 4008–4014.
96 C. Gögelein, D. Wagner, F. Cardinaux, G. Nägele and S. U. Egelhaaf, *J. Chem. Phys.*, 2012, **136**, 015102.
97 J. Hansen, R. Uthayakumar, J. S. Pedersen, S. U. Egelhaaf and F. Platten, *Phys. Chem. Chem. Phys.*, 2021, **23**, 22384–22394.
98 C. Haas, J. Drenth and W. W. Wilson, *J. Phys. Chem. B*, 1999, **103**, 2808–2811.
99 S. Ruppert, S. I. Sandler and A. M. Lenhoff, *Biotechnol. Prog.*, 2001, **17**, 182–187.
100 R. A. Curtis, H. W. Blanch and J. M. Prausnitz, *J. Phys. Chem. B*, 2001, **105**, 2445–2452.
101 E. Ruckenstein and I. L. Shulgin, *Adv. Colloid Interface Sci.*, 2006, **123–126**, 97–103.
102 O. Annunziata, A. Payne and Y. Wang, *J. Am. Chem. Soc.*, 2008, **130**, 13347–13352.
103 I. L. Shulgin and E. Ruckenstein, *J. Phys. Chem. B*, 2008, **112**, 14665–14671.
104 T. L. Hill, *An Introduction to Statistical Thermodynamics*, Addison-Wesley, Reading, 1960.
105 D. A. McQuarrie, *Statistical mechanics*, Harper & Row, New York, 1975.
106 D. Kashchiev, *Nucleation: Basic Theory with Applications*, Butterworth Heinemann, 2000.
107 C. N. Nanev, *J. Appl. Cryst.*, 2017, **50**, 1021–1027.
108 C. N. Nanev, *Prog. Cryst. Growth Charact. Mater.*, 2020, **66**, 100484.
109 M. Grant, *J. Cryst. Growth*, 2000, **209**, 130–137.
110 S. Jiang and J. H. ter Horst, *Cryst. Growth Des.*, 2011, **11**, 256–261.
111 R. P. Sear, *CrystEngComm*, 2014, **16**, 6506–6522.
112 O. Galkin and P. G. Vekilov, *Proc. Natl. Acad. Sci. U. S. A.*, 2000, **97**, 6277–6281.
113 P. G. Vekilov, *Nanoscale*, 2010, **2**, 2346–2357.
114 M. Sleutel and A. E. S. Van Driessche, *Proc. Natl. Acad. Sci. U. S. A.*, 2014, **111**, E546–E553.
115 A. Sauter, M. Oelker, G. Zocher, F. Zhang, T. Stehle and F. Schreiber, *Cryst. Growth Des.*, 2014, **14**, 6357–6366.
116 A. Sauter, F. Roosen-Runge, F. Zhang, G. Lotze, R. M. J. Jacobs and F. Schreiber, *J. Am. Chem. Soc.*, 2015, **137**, 1485–1491.
117 J. Drenth, K. Dijkstra, C. Haas, J. Leppert and O. Ohlenschläger, *J. Phys. Chem. B*, 2003, **107**, 4203–4207.
118 R. L. Davidchack and B. B. Laird, *Phys. Rev. Lett.*, 2000, **85**, 4751–4754.
119 S. Auer and D. Frenkel, *Nature*, 2001, **409**, 1020–1023.
120 R. P. Sear, *J. Phys. Chem. B*, 2006, **110**, 21944–21949.
121 V. Bhamidi, S. Varanasi and C. A. Schall, *Langmuir*, 2005, **21**, 9044–9050.
122 A. Nadarajah, E. L. Forsythe and M. L. Pusey, *J. Cryst. Growth*, 1995, **151**, 163–172.
123 K. Kurihara, S. Miyashita, G. Sazaki, T. Nakada, Y. Suzuki and H. Komatsu, *J. Cryst. Growth*, 1996, **166**, 904–908.
124 H. Hondoh and T. Nakada, *Cryst. Growth Des.*, 2008, **8**, 4262–4267.
125 S. Gorti, E. L. Forsythe and M. L. Pusey, *Cryst. Growth Des.*, 2004, **4**, 691–699.
126 S. Gorti, E. L. Forsythe and M. L. Pusey, *Cryst. Growth Des.*, 2005, **5**, 473–482.
127 Y. Saito, *Statistical Physics of Crystal Growth*, World Scientific, 1996.

